

Article

Starspot Activity without Pulsation in the Binary System KIC 5444392 Revisited

Mengqi Jin ^{1,2,†} , Jianning Fu ^{1,2,*} , Jiaxing Wang ^{3,†} and Weikai Zong ^{1,2,†}¹ Institute for Frontiers in Astronomy and Astrophysics, Beijing Normal University, Beijing 102206, China² Department of Astronomy, Beijing Normal University, No. 19, XinJieKouWai St., Beijing 100875, China³ School of Science, Chongqing University of Posts and Telecommunications, Chongqing 400065, China

* Correspondence: jnfu@bnu.edu.cn

† These authors contributed equally to this work.

Abstract: We revisited the short-period (~ 1.5 days) binary system KIC 5444392, which shows quasi-period modulated light variations. Previous studies indicated that these variations might be caused by stellar pulsations. In our work, we used the PHOEBE program, which revealed that this binary is an almost circular ($e \approx 0.007$) detached system with two G-type stars. The masses and radii of the primary and secondary stars were obtained as $M_1 = 1.21 \pm 0.06 M_\odot$, $R_1 = 1.69 \pm 0.09 R_\odot$ and $M_2 = 1.27 \pm 0.06 M_\odot$, $R_2 = 1.69 \pm 0.09 R_\odot$, respectively. Based on these parameters, the isochrone fitting showed that this system consists of a subgiant and a main-sequence star, whose ages are $3.89^{+0.37}_{-0.34}$ Gyr. Neither the primary nor the secondary star is in the mass range of Cepheid and Gamma Dor. Fourier analysis showed that the fitting residuals varied stochastically in a frequency around the orbital frequency, which means that the quasi-periodic signals resulted from starspots rather than stellar pulsation. Similar stellar parameters of both components of KIC 5444392 and the frequency analysis lead us to believe that starspots are in both stars. The autocorrelation analysis on the residuals indicates that the decay timescale of the starspots is about 53 days, and the rotational periods of both stars are very close to the orbital period of the binary. This result adheres to the trend that the decay timescale increases following the rotational frequency. Thus, studying this binary could increase our understanding of the light variations in the binary system.



Citation: Jin, M.; Fu, J.; Wang, J.; Zong, W. Starspot Activity without Pulsation in the Binary System KIC 5444392 Revisited. *Universe* **2023**, *9*, 417. <https://doi.org/10.3390/universe9090417>

Academic Editor: Sergei B. Popov

Received: 19 July 2023

Revised: 9 September 2023

Accepted: 9 September 2023

Published: 12 September 2023

Keywords: eclipsing binary; starspots; stellar rotation

1. Introduction

A multitude of magnetic phenomena are generated as a result of stellar rotation coupled with convective motions, including starspots and flares. These phenomena provide a rare opportunity to reveal the nature of stellar dynamos [1]. Since starspots can cause brightness variations by rotational modulation, a large amount of data has been collected for different types of stars [1]. Eclipsing binary systems offer a powerful method with which to study starspot activity on a star's surface, according to the light curve variations [2]. With the development of technology, data from photometry and spectroscopy support the analysis of binary systems to obtain precise absolute parameters such as masses, radii, and rotational periods [3], and to derive starspots' decay timescale [4,5].

Massive data are obtained via surveys such as the NASA *Kepler* mission [6] and the Transiting Exoplanet Survey (TESS) [7] which provide high-precision time-series photometry, and the Large Area Multi-Object Spectroscopic Telescope (LAMOST), which is located in the Xinglong Station of the National Astronomical Observatory, China, provides millions of spectra [8–10]. The LAMOST–*Kepler* project was proposed, providing follow-up spectroscopic observations for the objects in the *Kepler* field since 2012, and it obtained 766425 low-resolution spectra (LRS) until 2020 June [11]. In addition, the LAMOST–*Kepler* medium-resolution survey (LK-MRS; [12]) has also been conducted, starting in 2018. Thus,



Copyright: © 2023 by the authors. Licensee MDPI, Basel, Switzerland. This article is an open access article distributed under the terms and conditions of the Creative Commons Attribution (CC BY) license (<https://creativecommons.org/licenses/by/4.0/>).

combining these spectroscopy and photometry data provides a very advantageous way to study the characteristics of eclipsing binaries in the *Kepler* field.

KIC 5444392 is an eclipsing binary system with an orbital period of 1.5195284 ± 0.0000019 days in the *Kepler* field. In addition to the binary signal, it also shows out-of-eclipse variations. Based on the O-C diagram obtained from the *Kepler* Q0 to Q9 data, Giles et al. (2012) [13] diagnosed the variations with a high possibility of starspots. Meanwhile, in the research of Lei et al. (2022) [14], it was found that the primary star should be located in the classical Cepheid instability strip and should demonstrate pulsations (period range from 1 day to 50 days). Therefore, a detailed analysis is needed to better understand whether the variations originate from starspot modulations.

We describe the data of KIC 5444392 in Section 2. The binary modeling is shown in Section 3, and in Section 4, we analyze the quasi-periodic variations of the light curves after the binary modeling. Sections 5 and 6 discuss the results and present the conclusions, respectively.

2. Data Collection

2.1. Photometric Data

KIC 5444392 was observed by both *Kepler* and TESS. For data from *Kepler*, we obtained 18 long-cadence (LC) quarters and 4 short-cadence (SC) quarters, with cadences of 29.42 min and 59 s, respectively [6,15,16]. The aperture contamination factors were nearly 0 ($0.000, 9.000 \times 10^{-4}$) in all quarters. As for TESS, three sectors of data were obtained in 2 min mode. Detailed information about the data is listed in Table 1. In our work, the data for modeling binary light curves were downloaded from MAST. The PDCSAP flux is used because it is processed by the Presearch Data Conditioning (PDC) module [17], which corrects the raw data’s discontinuities, systematic trends, and outliers. However, long-time trends still exist in the light curves. To remove their influences, we applied a polynomial fitting for each quarter. Examples of light curves are shown in the left panel of Figure 1 using the data of *Kepler* LC Q5 after detrending. Meanwhile, the right panel of Figure 1 shows the phase-folded light curve based on the orbital period and BJD_0 provided by the *Kepler* Eclipsing Binary Catalogue (KEBC; [6,15]).

Table 1. The photometric observation information of KIC 5444392.

Telescope	Mode	Quarter/Sector	Precision (Mag)	Start Date (BJD)	End Date (BJD)
Kepler	LC	Q0~Q17	0.000376	2,454,953.539	2,456,424.002
Kepler	SC	Q1, Q3, Q9, Q10	0.000209	2,454,964.503	2,455,833.279
TESS	2 min mode	S14, S40, S41	0.00159	2,458,683.357	2,459,446.581

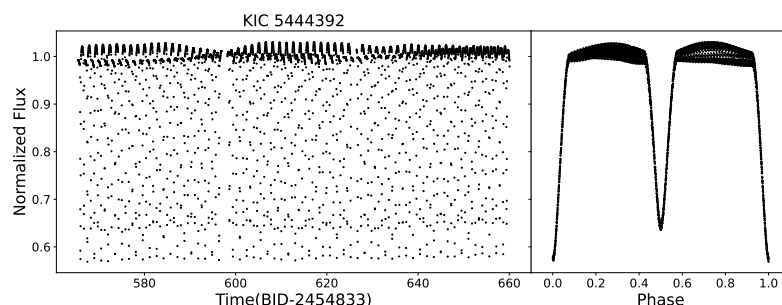


Figure 1. Light curves of KIC 5444392 observed by *Kepler* Q5. The flux is normalized by the mean value of the out-of-eclipse variations. The abscissas of the left and right panels are time and phase, respectively.

2.2. Spectroscopic Data

Spectroscopic observations of KIC 5444392 were made with LAMOST both in low- and medium-resolution modes. The spectral resolutions for the low- and medium-resolution

gratings are ~ 1800 and ~ 7500 , respectively [10,18]. Spectra of LRS with high S/N (average S/N is 225.68) were obtained to determine the atmospheric parameters of KIC 5444392 of $T_{\text{eff}} = 5955.62 \pm 20$ K, $\log g = 4.116 \pm 0.032$ dex, and $[\text{Fe}/\text{H}] = 0.051 \pm 0.013$ dex. More than 50 spectra of MRS were obtained with the average S/N = 105.66. The spectroscopic observations are listed in Table 2, and the detailed information is listed in Table A1. According to the method of Zhang et al. (2021) [19], the radial velocities (RVs) of KIC 5444392 were extracted. They used the cross-correlation function (CCF) [20] to select the best-matched template and adopted the corresponding RV as the initial guess of the final RV. The final RV was determined by maximizing the CCF using the optimization routine `scipy.optimize.minimize` via the Nelder–Mead algorithm [21]. The measurement errors were obtained via the Monte Carlo method, in which this method was repeated 100 times, and each time, a Gaussian random noise was added according to the flux error. The RV curve is shown in Figure 2. From the MRS, one may note that KIC5444392 is a double-lined spectroscopic binary (SB2). We used the Keplerian orbital equation to fit the RV curve. The semi-amplitudes K_1 , K_2 , eccentricities e , pericenter ω , and system barycentric velocities γ_0 are derived and listed in Table 2. The best-fitting curves are shown in Figure 2. The mass ratio of KIC 5444392 is derived as $q = K_2/K_1 = 0.955 \pm 0.002$.

Table 2. The spectroscopic observations of KIC 5444392 and the derived stellar parameters of the primary star.

Mode	Wavelength Coverage	Number of Observations	Average S/N	Teff	[Fe/H]	log g
LRS	370 nm~900 nm	2	225.68	5955.62 ± 20 K	0.051 ± 0.013	4.116 ± 0.028
MRS	495–535 nm (B) and 630–680 nm (R)	102	105.66	\	\	\

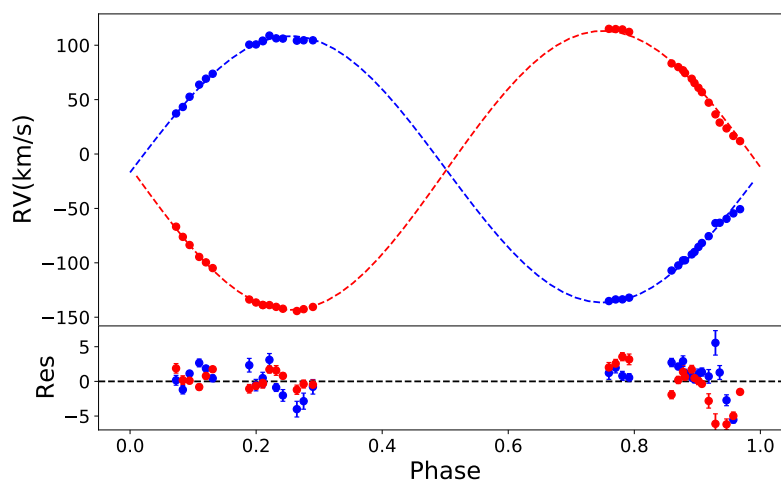


Figure 2. The RV curve of KIC5444392 is shown in the top panel. The blue dots represent the observed RVs of the primary and the red dots represent those of the secondary. The best-fitting curves are shown with dashed lines. The bottom panel shows the corresponding residuals.

3. Binary Modeling Revisited

Binary modeling can be a valid way to obtain the absolute parameters for a binary system. The code we applied is the physics of eclipsing binaries (PHOEBE 2.2; [22–24]) code, which makes improvements to the precise *Kepler* data [25] based on the Wilson–Devinney code (WD code) [26].

The entire procedure is listed below:

- (i) The Gaussian process (GP) method [27] is used to model the out-of-eclipse quasi-sinusoidal signals. Since the signals of binary eclipsing and quasi-sinusoidal are mixed in the light curves, one needs to subtract the latter before performing the binary modeling.

One of the crucial steps in the GP method is searching for an appropriate GP kernel. The kernel used in this work is provided by [28] and described as follows:

$$k_{ij} = A \exp \left[-\frac{(t_i - t_j)^2}{2l^2} - \Gamma^2 \sin^2 \left(\frac{\pi(t_i - t_j)}{P} \right) \right] + \sigma^2 \delta_{ij} \tag{1}$$

where k_{ij} is the covariance between the i th and the j th data, while t_i and t_j are the epochs of the i th and the j th data, respectively. Here, A , l , P , and σ are free parameters.

(ii) The quasi-sinusoidal signals are subtracted to derive the binary signals.

(iii) The PHOEBE code is used to model the binary signals of one quarter to obtain the initial modeling parameters. The mass ratio q , the primary temperature T_1 , and the orbital period P_{orb} are fixed as 0.955, 5955.62 K, and 1.5195284 days, respectively. The inclination i , the primary mass M_1 , the primary radius R_1 , the secondary radius R_2 , the secondary effective temperature T_2 , the eccentricity of the binary e , and the arguments of the pericenter ω are free parameters. During the modeling, a trial of Markov chain Monte Carlo (MCMC) sampling is used to adjust the bounds for each free parameter.

(iv) A series of iterations is performed from step (i) to step (iii) to identify the optimal solution for the quarter of light curves of binary eclipsing.

(v) The optimal solution is used as the initial solution for the remaining quarters and the same iterations are performed to obtain the optimal solution for each quarter.

(vi) All the optimal solutions are collected to obtain the best-fitting model and calculate the error in each parameter.

The orbital solution and uncertainties are summarized in Table 3. The best-fitting light curves and the residuals can be found in Figure 3. We compared our work to that of Lei [14]; the parameters are all consistent except for the masses and radii, which have a slight difference but are still within the error range. This difference is acceptable as we applied the GP process to deal with the light curve before modeling, while this step was not used in the work of Lei et al. [14].

Table 3. Orbital solution and physical parameters of KIC 5444392.

Parameter	Primary	System	Secondary
BJD ₀		2,454,954.915115 ± 0.031633	
P_{orb} (day)		1.5195284	
e		0.007 ± 0.001	
K_1 (km/s)		122.51 ± 0.24	
K_2 (km/s)		128.30 ± 0.21	
γ_0 (km/s)		−14.55 ± 0.08	
ω (deg)		53.90 ± 12.61	
q (M ₁ /M ₂)		0.955	
i (deg)		84.54 ± 0.16	
a (R _⊙)		7.55 ± 0.1	
Mass (M _⊙)	1.21 ± 0.06		1.27 ± 0.06
Radius (R _⊙)	1.69 ± 0.09		1.69 ± 0.09
Teff (K)	5955.62 ± 20		5730 ± 10
log g (cgs)	4.05 ± 0.02		4.03 ± 0.02
Gravity-darkening exponent	0.32		0.32

By fitting the mass and radii of the two components with Padova isochrones [29], we determined the binary system age of KIC 5444392. The fitting results are shown in Figure 4. The logarithm of the age of the system is estimated to be $\log t = 9.59^{+0.04}_{-0.04}$. The best-fitting $\log t$'s of the primary and secondary are 9.55 and 9.63 dex, respectively. The isochrones show that the primary is a subgiant star and the secondary is a main-sequence star. In addition, these two components are near the main-sequence turn-off. The primary star evolves a bit faster than the secondary star.

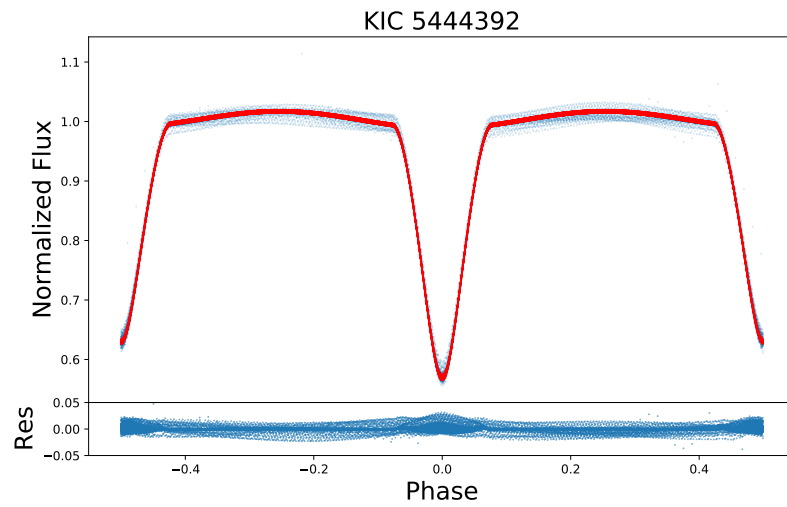


Figure 3. The best fit of the light curve of KIC 5444392. The upper panel shows the phase-folded light curves of KIC 5444392 with the blue points for the data from Kepler LC Q5 and the red curve being the best-fitting model from PHOEBE. The bottom panel shows the residuals.

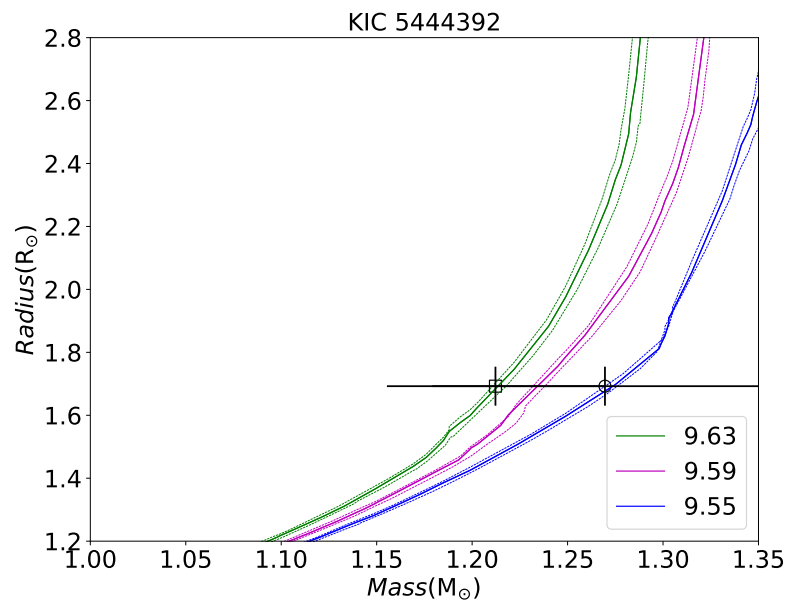


Figure 4. The fitting isochrones of KIC 5444392. The square and circle denote the locations of the primary and secondary, respectively. The solid lines show the isochrones with metallicity of $[Fe/H]$, which is 0.051 derived from the spectra. The color of the line represents the logarithm of the age of the binary system $\log t$. The dashed lines show the isochrones with metallicity of $[Fe/H] \pm \sigma_{[Fe/H]}$, which are 0.051 ± 0.013 .

4. Analyzing the Out-of-Eclipse Signals

4.1. Frequency Analysis

Either stellar pulsations or starspots with rotational modulation could cause quasi-periodic signals. In order to make a judgment, we applied a Fourier transform to the residuals to analyze the periodic signals. Since the LC data have a cadence of around 30 min, frequencies larger than 24 c/d can be filtered out. Therefore, the SC data were also analyzed separately to check signals with high frequencies. In order to determine whether the pulsations occurred after the *Kepler* observations, the TESS data were also analyzed. The quasi-periodic signals were extracted by subtracting the binary modeling, and shown in Figure 5 is an example which used the LC data. The frequency spectra of the LC, SC, and TESS data can be found in the upper, middle, and lower panels of Figure 6, respectively.

All three spectra reveal that the main frequency is close to the binary orbit frequency (black dashed lines) and the rotation period (red dashed lines). It can be clearly seen in the middle panel of Figure 6 that there is no signal except for the harmonic rotational frequencies in the high-frequency region. The width of the spectral window is smaller than the difference between the rotational period and the orbital period, which means the two periods are separated. Also, the sidelobe of the spectral window for LC is quite clean and should not affect the frequency spectrum. Thus, the signals are unlikely to originate from stellar pulsations. In addition, the mass and radii we derived from binary modeling show neither the primary nor the secondary star are in the mass range of Cepheid and Gamma Dor. Accordingly, we prefer to believe that starspots are the reason for the light curve variations of KIC 5444392.

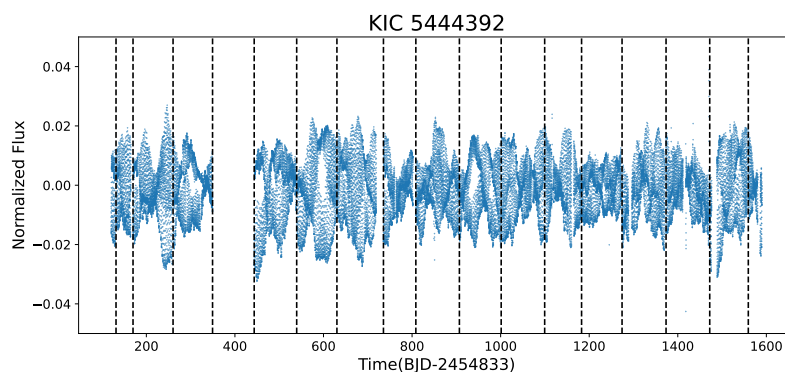


Figure 5. Out-of-eclipse flux residuals of KIC5444392 from Kepler data. The data for quarter 4 were discarded due to their poor quality.

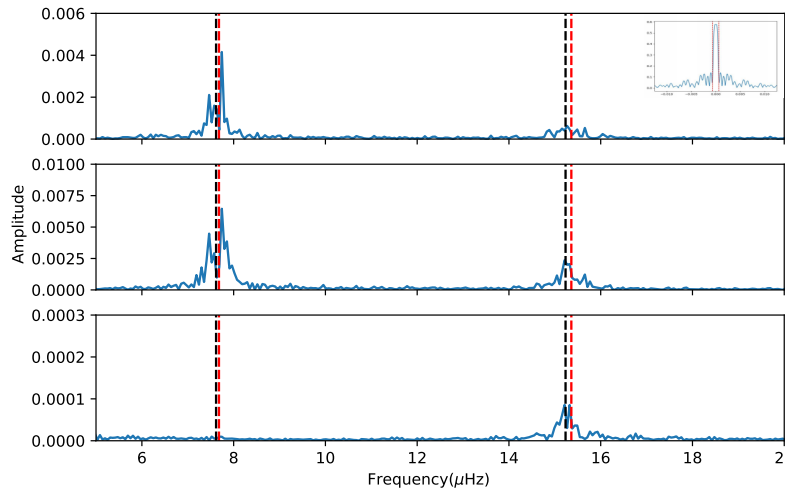


Figure 6. The frequency spectra of residuals from *Kepler* LC, *Kepler* SC, and TESS are shown in the upper, middle, and lower panels, respectively. The first and second black dashed lines show the frequencies that correspond to the orbital period and its first harmonic frequency, respectively. The first and second red dashed lines stand for the frequencies related to the average rotational period and its first harmonic frequency, respectively. The spectral window for LC data is shown in the upper right corner.

A sliding Fourier transform with a window width of 180 days and a step of 1 day is performed on the LC data [30,31]. The time-period diagram is shown in Figure 7. The main period has stochastic variations near the orbital frequency and its amplitude varies randomly. The random emergence and decay of starspots could be appropriate to explain the stochastic behavior of the main period signals. Therefore, the quasi-periodic signals appear to be caused by starspots.

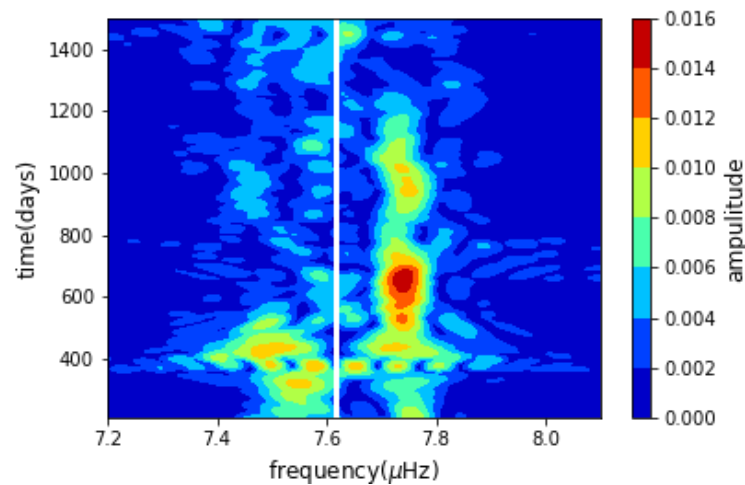


Figure 7. Sliding Fourier transform diagram. The color represents the amplitude of the signal. The white vertical line indicates the orbital frequency.

4.2. Starspot Analysis

Starspots are commonly observed in binary systems, especially in late-type stars [32]. The residuals of binary light curves with quasi-sinusoidal periodic variations contain information about the rotation period, the decay timescale, and the evolution of active regions [5].

Using the autocorrelation function (ACF) method [2,33], we can derive the starspot parameters, as the ACF represents the degree of self-similarity of starspot signals over time lag. The behavior of the ACF is similar to the underdamped simple harmonic oscillator (uSHO) at lower time lags [2]. Thus, the core equation used to fit the ACF is shown as follows:

$$y(t) = e^{(-t/\tau_{AR})} \left[A \cos\left(\frac{2\pi t}{P}\right) + B \cos\left(\frac{4\pi t}{P}\right) + y_0 \right] \quad (2)$$

where τ_{AR} , P , A , B , and y_0 stand for the decay timescale of the ACF, the stellar rotation period, the amplitudes of the cosine terms, and the offset, respectively [2]. The equation shows that when the time lag is close to integral multiples of the stellar rotation period, the correlation becomes stronger and the ACF presents a peak. As the time lag increases, the amplitude of the peak decreases, meaning that the decay rate of the amplitude of the peak represents the decay timescale of the starspots [2].

To obtain the best fitting of starspots, we fit the ACF using the EMCEE code to the residuals, which are rebinned every four quarters and the whole observation time. The fitting results show that the decay timescale is about 33.3–70.8 days and the rotation period is about 1.498–1.526 days close to the orbital period $P_{orb} = 1.5195284$ days. An example of the results is shown in Figure 8, which displays the ACF of the starspots, and the corresponding best-fitting MCMC results are shown in Figure 8 as an example. The fitting results of the starspot parameters are listed in Table 4.

To better understand the features of starspots, we use the duration and depth of dips and the single-/double-dip ratio (SDR) as shown in [34] to describe the characteristics. The starspot signals present one or two dips in each rotation. A dip with a duration between 0.2 and 0.8 rotations is considered as a double dip; otherwise, it is considered a single dip. The duration of the dip is the distance between two adjacent peaks around the dip and the depth of the dip is the flux difference between the higher peak and the dip [35]. The results are shown in Figure 9. The SDR is around -0.15 , revealing that the starspots are dominated by double dips.

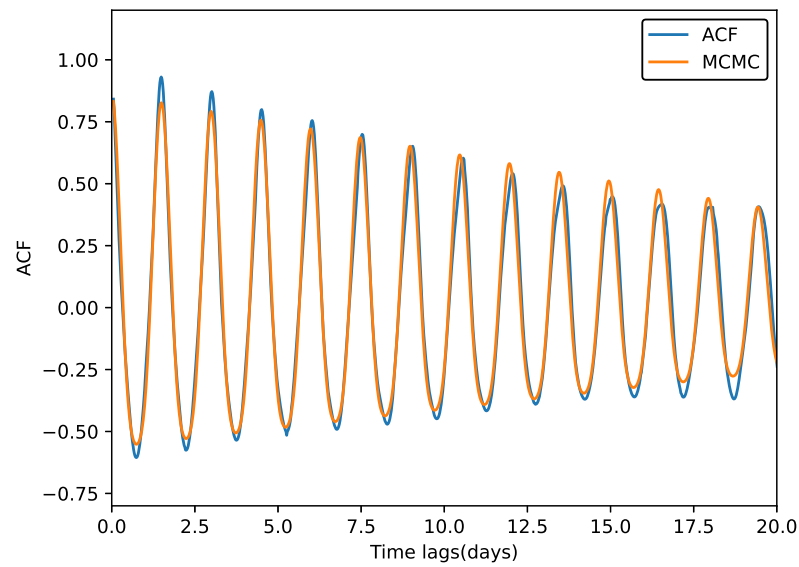


Figure 8. The ACF of KIC 5444392 of Q10~Q13. The blue curve represents the ACF signal and the orange curve represents the uSHO model.

Table 4. The parameters of starspots.

Bin	τ (day)	A	B	P_{rot} (day)	y_1
Q1~Q4	52.422154 ± 0.0144	0.680993	0.066364	1.500624	-0.004941
Q2~Q5	70.224692 ± 0.106152	0.796998	0.087727	1.514044	0.0083
Q3~Q6	70.765516 ± 0.0457055	0.936271	0.076179	1.504925	0.041158
Q6~Q9	60.87793 ± 0.013099	0.68487	0.09419	1.49805	0.105345
Q7~Q10	63.302944 ± 0.0589405	0.799516	0.07408	1.498034	0.066511
Q8~Q11	63.638247 ± 0.1615685	0.905104	0.048307	1.500012	0.024062
Q9~Q12	70.114559 ± 0.0658885	0.79399	0.051991	1.506741	0.013049
Q10~Q13	36.764739 ± 0.010291	0.712457	0.12586	1.495144	0.023537
Q11~Q14	33.312171 ± 0.029439	0.558335	0.221856	1.503421	0.127531
Q12~Q15	38.371631 ± 0.0743795	0.431974	0.157616	1.516189	0.15008
Q13~Q16	46.128176 ± 0.0057205	0.636023	0.070252	1.52191	0.107329
Q14~Q17	48.046861 ± 0.0848265	0.757974	0.041402	1.526177	0.090904
Average	53.1322774 ± 0.0558675	0.7216514	0.0961733	1.5070603	0.0749506

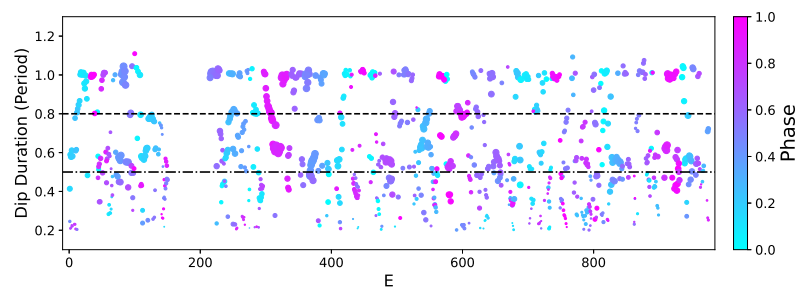


Figure 9. The dip duration varies with the rotational cycle. The size of the circle represents the depth of the dip. The phase of the dip is indicated by the colors. The dot-dashed line represents the dip duration of a half period. The bound of single and double dips is shown in the dashed line.

5. Discussion

5.1. The O-C Diagram

In research on the hierarchical triple candidates of [13], the O-C values of KIC 5444392 with data from *Kepler* LC Q0 to Q9 have been calculated, and a period change rate $\dot{P} / P = -0.68 \times 10^{-6} \text{ year}^{-1}$ has been obtained. However, their O-C diagram of KIC 5444392 presents quasi-periodic variations rather than parabolic or sinusoidal shapes.

Thus, the researchers considered that the change originated from the starspot prograde, since the rotation is a little faster than the orbital motion.

Based on the TESS data, the observation baseline of KIC 5444392 is about 3000 days, providing a good opportunity to recheck the eclipse timing variations. Combining all the data available, we plotted the new O-C diagram of this binary, which is shown in Figure 10. It can be seen that the O-C values increased with the epoch. Since the starspot caused significant dispersion, the shape of the trend could not be determined for certain. We adopted the linear and quadratic curves to fit the data and obtained the variance of residuals, calculated as:

$$\sigma^2 = \frac{1}{N} \sum_{i=1}^N [m_i - G(t_i)]^2 \tag{3}$$

where $G(t)$ is defined as

$$G(t) = [g_1(E), g_2(E)] \begin{cases} g_1(E) = aE + b \\ g_2(E) = aE^2 + bE + c \end{cases} \tag{4}$$

Here, N stands for the number of data points, while m_i presents the calculated value of O-C. The fitting parameters are listed in Table 5 and can be determined based on the curves shown in Figure 10.

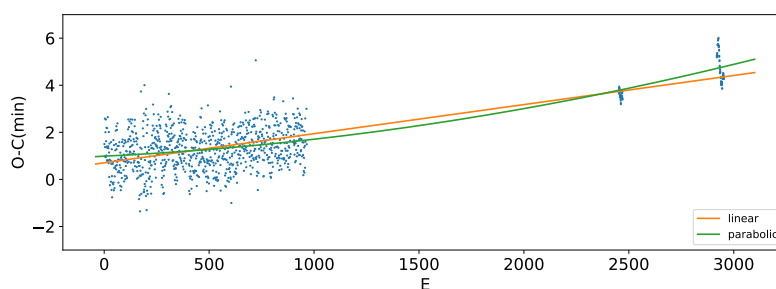


Figure 10. The O-C diagram of KIC 5444392 with the data from *Kepler* and TESS. Two different fittings are used to derive the period changes; they are shown in orange and red for the linear and parabolic fitting, respectively.

Table 5. Fitting results of the O-C values.

Fitting Equation	Parameters		
	a	b	c
$g_1(t)$	1.25×10^{-3}	7.06×10^{-1}	
$g_2(t)$	2.90×10^{-7}	4.31×10^{-4}	9.86×10^{-1}

To determine the better-fitting curve, we utilized the statistical test described by Pringle [36], which defines λ as

$$\lambda = \frac{(\sigma_1^2 - \sigma_2^2) / (D_2 - D_1)}{\sigma_2^2 / (N - D_2)} \tag{5}$$

Here, D_i is assigned a value of two or three for linear or quadratic fitting, respectively, as the degree of freedom of the fitting equation. A significant improvement for the higher degree of freedom fitting should have the parameters that meet the F-distribution, $\lambda > FP_{-99.75\%}(D_2 - D_1, N - D_2)$ [37]. After checking the F values, we find the linear fitting is better. Therefore, the orbital period and BJD_0 should be corrected with 8.65×10^{-7} days and 4.9×10^{-4} days, respectively. These corrections have uncertainties of 1.9×10^{-6} and 0.031633 days, respectively. The long baseline of observations reveals the accurate orbital

period is 1.5195201 days and BJD_0 is 245,4954.985605. However, as the time coverage of the data is quite short, the results of the O-C diagram should be updated if more observation data are obtained.

5.2. Possibility of Stellar Pulsations

As demonstrated by the frequency analysis in Section 4.1 and the O-C diagram in Section 5.1, the quasi-periodic signals appear to result from the starspot activities. However, Lei [14] considered that the variations are classical Cepheid pulsations because the primary star is located in the classical Cepheid instability strip.

Based on our results, the primary star could not be regarded as a Cepheid pulsator. Its small variation amplitude (~ 0.002 mag) and the mass of $1.21 M_{\odot}$ show that it could not be a classical Cepheid, which have variation amplitudes between 0.1 mag and 2 mag with a mass larger than $3 M_{\odot}$. Also, its $[Fe/H] = 0.051 \pm 0.013$ revealed that the star could not be a Cepheid of stellar population II. Therefore, the variations were more likely to have been caused by starspot signals.

5.3. Comparing the Starspot Properties with Those of Other Works

The decay timescale of the starspot of KIC 5444392 is 53 days, which is consistent with that of the single star with the same effective temperature described by [2], who presented a sample of single stars with rotational periods near 10 days and 20 days, for which the timescale decreased with the rotational period. Baris [38] measured the variation in the decay timescale with the rotational period. Their single star sample has a wide rotational period range from 3 to 50 days. Comparing their result with ours, the decay timescale of starspots of KIC 5444392 is in the range of their trend. However, Baris [38] showed that the dispersal increases significantly as the rotational period decreases, rendering the decay timescale of the starspots of KIC 5444392 longer than that of most single stars. We could not determine if the binary interaction affected the evolution of starspots. Compared with the binary sample collected by Wang [35], the timescale of KIC 5444392 was consistent with that of this sample, confirming the conclusion that the timescale increases as the rotational period decreases.

The rms of starspot signals is adopted as a proxy of the size of starspots; for KIC 5444392 the rms is 0.01. This rms value is consistent with that of the sample of binaries of Wang [35]. This rms also indicates that the rms increases as the rotational period decreases. This rms is also larger than that of the starspots of single stars, with the same effective temperature of the sample of Giles et al. (2017) [2]. Since the rotational period is 1.5 days, which is shorter than the 10-day rotational period of the single-star sample, this result is reasonable.

The SDR of KIC 5444392 is -0.15 . Compared with that of the binary sample of Wang [35], this signal shows a smaller SDR than those with the same decay timescales, which means that most of the signals have two dip patterns. This system has two similar components, and both should show a similar amplitude of starspot modulation in the light curves. The complex configuration of starspots generally results in two dip patterns. Compared with the single star model of Baris [34], this SDR value is in the range of the single-star model and near the bottom bound.

In general, the starspot properties of KIC 5444392 are consistent with those observed in other works. However, due to the short period of this binary system, no similar samples (obtained during periods of less than 3 days) were found in the literature, preventing a comparison of the results. This could be improved upon in future studies.

6. Conclusions

Combining the photometric data from Kepler and TESS with the spectroscopic data from LAMOST, we revisited the detached binary system KIC5444392. Precise stellar parameters were obtained via binary modeling using the PHOEBE code. Compare with other works, we observed a slight difference in mass and radii which was caused by

different binary modeling methods; in particular, we took the starspots into consideration prior to the modeling. KIC 5444392 consists of two G-type stars with masses and radii of $M_1 = 1.21 \pm 0.06 M_\odot$, $R_1 = 1.69 \pm 0.09 R_\odot$ and $M_2 = 1.27 \pm 0.06 M_\odot$, $R_2 = 1.69 \pm 0.09 R_\odot$, respectively. The ratio of the radii could be derived from the spectra. However, due to the ratio of the radii from spectra being given by the stellar model, it is not as accurate as the mass ratio and depends on the model. Secondly, the amplitude of the radial velocity is relatively large, hence it may be difficult to fit the spectrum in practice because each star has a drag effect and widens the spectrum. This difference may affect the parameters of the two stars. The parameters we obtained from the binary modeling are capable of restoring the light curve. But we cannot rule out other parametric solutions. The tiny eccentricity shows that the binary system has a nearly circular orbit. The age of the binary system derived from the isochrones fitting is $3.89^{+0.37}_{-0.34}$ Gyr.

In addition to the eclipsing signals, the light curves also show signals which could originate from either pulsations or starspots. We use frequency analysis to derive the periods of the residuals. Combined with the periods and the stellar parameters obtained from the binary modeling, we exclude the possibility of pulsations.

For starspots, the power spectrum did not clearly show two separated frequencies and the physical parameters of the two components are very similar, thus both stars have starspots and have been synchronized. We use the EMCEE code to carry out the ACF method in order to obtain the starspot parameters. The average rotation period is 1.507 days, which is close to the orbit period. The decay timescale of the starspots is about 53 days, which is consistent with that of the starspots of other binaries. The SDR of the residuals is -0.15 , implying that the starspot activity of KIC 5444392 during the total duration time are dominated by double dips. According to the derived stellar parameters and the estimated rotational period, the breakup velocity of the primary star is around 362 km/s and the equatorial velocity is around 59 km/s, the breakup velocity of the secondary star is around 373 km/s and the equatorial velocity is around 59 km/s, both equatorial velocities are smaller than the breakup velocities. Therefore, both stars of KIC 5444392 are stable. And also, due to the rotational period of KIC 5444392 being very close to the binary orbital period, the binary system is nearly tidally locked.

The study of this binary system reminds us that more detailed research should be conducted to determine whether the small variations in the light curve are caused by starspots or pulsation. Also, to study the details of starspots, long-baseline high-quality multiband photometric data are required.

Author Contributions: Methodology, J.W.; Writing—original draft, M.J.; Writing—review, editing, J.F. and W.Z. All authors have read and agreed to the published version of the manuscript.

Funding: This research was funded by the National Natural Science Foundation of China (NSFC) grant number 11833002, 12090040, 12090042, and 12203010.

Data Availability Statement: The data underlying this article will be shared on reasonable request to the corresponding author.

Acknowledgments: We acknowledge the support of the NSFC. The Guoshoujing Telescope (the Large Sky Area Multi-Object Fiber Spectroscopic Telescope, LAMOST) is a National Major Scientific Project built by the Chinese Academy of Sciences. Funding for the project was provided by the National Development and Reform Commission. LAMOST is operated and managed by the National Astronomical Observatories, Chinese Academy of Sciences. We are very appreciate of Zhang Bo's assistance in this article. We thank the anonymous reviewers for their valuable comments that greatly improved the manuscript.

Conflicts of Interest: The authors declare no conflict of interest.

Appendix A

Table A1. Detailed information of the spectroscopic data from LAMOST. The obsid is the unique number ID of this spectrum in LAMOST and the lmjd is the local modified Julian day.

Obsid	LRS/MRS	Obsdate	Lmjd	Band	SNR	Obsid	LRS/MRS	Obsdate	Lmjd	Band	SNR
52415214	LRS	2012/6/15	56094	G	133.07	826701102	MRS	2020/6/3	59004	B	66.24
154001090	LRS	2013/5/19	56432	G	318.28	826701102	MRS	2020/6/3	59004	B	63.81
744801102	MRS	2019/5/21	58625	B	28.17	826701102	MRS	2020/6/3	59004	B	60.34
744801102	MRS	2019/5/21	58625	B	4.96	826701102	MRS	2020/6/3	59004	R	113.62
744801102	MRS	2019/5/21	58625	B	31.45	826701102	MRS	2020/6/3	59004	R	120.82
744801102	MRS	2019/5/21	58625	R	51.18	826701102	MRS	2020/6/3	59004	R	116.17
744801102	MRS	2019/5/21	58625	R	56.79	826701102	MRS	2020/6/3	59004	R	114.55
744801102	MRS	2019/5/21	58625	R	7.76	826701102	MRS	2020/6/3	59004	R	109.92
747001102	MRS	2019/6/9	58644	B	58.38	824801102	MRS	2020/6/5	59006	B	77.24
747001102	MRS	2019/6/9	58644	B	64.52	824801102	MRS	2020/6/5	59006	R	127.46
747001102	MRS	2019/6/9	58644	B	60.77	825601102	MRS	2020/6/10	59011	B	34.92
747001102	MRS	2019/6/9	58644	B	58.5	825601102	MRS	2020/6/10	59011	B	35.91
747001102	MRS	2019/6/9	58644	R	99.09	825601102	MRS	2020/6/10	59011	B	25.23
747001102	MRS	2019/6/9	58644	R	106.93	825601102	MRS	2020/6/10	59011	B	22.3
747001102	MRS	2019/6/9	58644	R	102.87	825601102	MRS	2020/6/10	59011	R	65.85
747001102	MRS	2019/6/9	58644	R	96.38	825601102	MRS	2020/6/10	59011	R	67.71
747401102	MRS	2019/6/11	58646	B	51.43	825601102	MRS	2020/6/10	59011	R	49.1
747401102	MRS	2019/6/11	58646	R	94.43	825601102	MRS	2020/6/10	59011	R	42.86
747401102	MRS	2019/6/11	58646	B	49.21	826101102	MRS	2020/6/14	59015	B	72.7
747401102	MRS	2019/6/11	58646	B	51.84	826101102	MRS	2020/6/14	59015	B	80.42
747401102	MRS	2019/6/11	58646	R	99.7	826101102	MRS	2020/6/14	59015	B	83.1
747401102	MRS	2019/6/11	58646	R	98.94	826101102	MRS	2020/6/14	59015	B	77.21
744801102	MRS	2019/5/21	58625	B	48.23	826101102	MRS	2020/6/14	59015	B	83.85
744801102	MRS	2019/5/21	58625	R	84.03	826101102	MRS	2020/6/14	59015	B	82.89
747001102	MRS	2019/6/9	58644	B	137.61	826101102	MRS	2020/6/14	59015	R	131.47
747001102	MRS	2019/6/9	58644	R	221	826101102	MRS	2020/6/14	59015	R	142.28
747401102	MRS	2019/6/11	58646	B	98.37	826101102	MRS	2020/6/14	59015	R	148.27
747401102	MRS	2019/6/11	58646	R	179.95	826101102	MRS	2020/6/14	59015	R	138.22
824301102	MRS	2020/5/31	59001	B	38.38	826101102	MRS	2020/6/14	59015	R	151.68
824301102	MRS	2020/5/31	59001	B	78.79	826101102	MRS	2020/6/14	59015	R	147.55
824301102	MRS	2020/5/31	59001	B	71.21	826401102	MRS	2020/6/15	59016	B	51.23
824301102	MRS	2020/5/31	59001	B	44.86	826401102	MRS	2020/6/15	59016	B	56.28
824301102	MRS	2020/5/31	59001	B	32.24	826401102	MRS	2020/6/15	59016	B	57.15
824301102	MRS	2020/5/31	59001	R	71.39	826401102	MRS	2020/6/15	59016	B	60.63
824301102	MRS	2020/5/31	59001	R	139.84	826401102	MRS	2020/6/15	59016	R	99.65
824301102	MRS	2020/5/31	59001	R	131.13	826401102	MRS	2020/6/15	59016	R	107.64
824301102	MRS	2020/5/31	59001	R	89.11	826401102	MRS	2020/6/15	59016	R	109.05
824301102	MRS	2020/5/31	59001	R	62.66	826401102	MRS	2020/6/15	59016	R	114.39
824501102	MRS	2020/6/2	59003	B	53.41	824301102	MRS	2020/5/31	59001	B	186.4
824501102	MRS	2020/6/2	59003	B	60.18	824301102	MRS	2020/5/31	59001	R	320.56
824501102	MRS	2020/6/2	59003	B	61.84	824501102	MRS	2020/6/2	59003	B	165.71
824501102	MRS	2020/6/2	59003	B	62.23	824501102	MRS	2020/6/2	59003	R	286.19
824501102	MRS	2020/6/2	59003	B	58.52	826701102	MRS	2020/6/3	59004	B	163.96
824501102	MRS	2020/6/2	59003	B	62.58	826701102	MRS	2020/6/3	59004	R	278.3
824501102	MRS	2020/6/2	59003	R	96.21	824801102	MRS	2020/6/5	59006	B	83.46
824501102	MRS	2020/6/2	59003	R	106.9	824801102	MRS	2020/6/5	59006	R	133.87
824501102	MRS	2020/6/2	59003	R	110.4	825601102	MRS	2020/6/10	59011	B	77.45
824501102	MRS	2020/6/2	59003	R	110.13	825601102	MRS	2020/6/10	59011	R	140.17
824501102	MRS	2020/6/2	59003	R	110.34	826101102	MRS	2020/6/14	59015	B	219.3
824501102	MRS	2020/6/2	59003	R	113.43	826101102	MRS	2020/6/14	59015	R	381.69
826701102	MRS	2020/6/3	59004	B	63.88	826401102	MRS	2020/6/15	59016	B	130.14
826701102	MRS	2020/6/3	59004	B	68.88	826401102	MRS	2020/6/15	59016	R	236.19

References

1. Berdyugina, S.V. Starspots: A Key to the Stellar Dynamo. *Living Rev. Sol. Phys.* **2005**, *2*, 1–62. [[CrossRef](#)]
2. Giles, H.A.C.; Collier Cameron, A.; Haywood, R.D. A Kepler study of starspot lifetimes with respect to light-curve amplitude and spectral type. *Mon. Not. R. Astron. Soc.* **2017**, *472*, 1618–1627. [[CrossRef](#)]
3. Pan, Y.; Fu, J.-N.; Zong, W.; Zhang, X.; Wang, J.; Li, C. Starspot Modulation Detected in the Detached Eclipsing Binary KIC 8301013. *Astrophys. J.* **2020**, *905*, 67. [[CrossRef](#)]
4. Helminiak, K.G.; Ukita, N.; Kambe, E.; Kozłowski, S.K.; Sybilski, P.; Ratajczak, M.; Maehara, H.; Konacki, M. HIDES spectroscopy of bright detached eclipsing binaries from the Kepler field—I. Single-lined objects. *Mon. Not. R. Astron. Soc.* **2016**, *461*, 2896–2913. [[CrossRef](#)]
5. Lurie, J.C.; Vyhmeister, K.; Hawley, S.L.; Adilia, J.; Chen, A.; Davenport, J.R.A.; Jurić, M.; Puig-Holzman, M.; Weisenburger, K.L. Tidal Synchronization and Differential Rotation of Kepler Eclipsing Binaries. *Astron. J.* **2017**, *154*, 250. [[CrossRef](#)]
6. Prša, A.; Batalha, N.; Slawson, R.W.; Doyle, L.R.; Welsh, W.F.; Orosz, J.A.; Seager, S.; Rucker, M.; Mjaseth, K.; Engle, S.G. Kepler Eclipsing Binary Stars. I. Catalog and Principal Characterization of 1879 Eclipsing Binaries in the First Data Release. *Astron. J.* **2011**, *141*, 83. [[CrossRef](#)]
7. Ricker, G.R.; Winn, J.N.; Vanderpek, R.; Latham, D.W.; Bakos, G.; Bean, J.L.; Berta-Thompson, Z.K.; Brown, T.M.; Buchhave, L.; Butler, N.R.; et al. Transiting Exoplanet Survey Satellite (TESS). *J. Astron. Telesc. Instrum. Syst.* **2015**, *1*, 014003. [[CrossRef](#)]
8. Wang, S.-G.; Su, D.-Q.; Chu, Y.-Q.; Cui, X.; Wang, Y.-N. Special configuration of a very large Schmidt telescope for extensive astronomical spectroscopic observation. *Appl. Opt.* **1996**, *35*, 5155–5161. [[CrossRef](#)]
9. Cui, X.; Wang, S.-G.; Su, D.-Q.; Zhao, Y.; Wang, Y.-N.; Chu, Y.; Li, G. Southern LAMOST for all sky spectroscopic survey. In *Ground-Based and Airborne Telescopes III*; SPIE: Washington, DC, USA, 2010; Volume 7733. [[CrossRef](#)]
10. Cui, X.-Q.; Zhao, Y.-H.; Chu, Y.-Q.; Li, G.-P.; Li, Q.; Zhang, L.-P.; Su, H.-J.; Yao, Z.-Q.; Wang, Y.-N.; Xing, X.-Z.; et al. The Large Sky Area Multi-Object Fiber Spectroscopic Telescope (LAMOST). *Res. Astron. Astrophys.* **2012**, *12*, 1197–1242. [[CrossRef](#)]
11. Fu, J.; Zong, W.; Wang, H. LAMOST-Kepler project and related scientific research. *Sci. Sin. Phys. Mech. Astron.* **2022**, *52*, 289502. [[CrossRef](#)]
12. Zong, W.; Fu, J.-N.; De Cat, P.; Wang, J.; Shi, J.; Luo, A.; Zhang, H.; Frasca, A.; Molenda-Żakowicz, J.; Gray, R.O.; et al. Phase II of the LAMOST-Kepler/K2 Survey. I. Time Series of Medium-resolution Spectroscopic Observations. *Astrophys. J. Suppl. Ser.* **2020**, *251*, 15. [[CrossRef](#)]
13. Gies, D.R.; Williams, S.J.; Matson, R.A.; Guo, Z.; Thomas, S.M.; Orosz, J.A.; Peters, G.J. A Search for Hierarchical Triples using Kepler Eclipse Timing. *Astron. J.* **2012**, *143*, 137. [[CrossRef](#)]
14. Lei, Y.; Li, G.; Zhou, G.; Li, C. Analysis of Five Double-lined Spectroscopic Eclipsing Binaries Observed with TESS and LAMOST. *Astron. J.* **2022**, *163*, 235. [[CrossRef](#)]
15. Kirk, B.; Conroy, K.; Prša, A.; Abdul-Masih, M.; Kochoska, A.; Matijević, G.; Hambleton, K.; Barclay, T.; Bloemen, S.; Boyajian, T.; et al. Kepler Eclipsing Binary Stars. VII. The Catalog of Eclipsing Binaries Found in the Entire Kepler Data Set. *Astron. J.* **2016**, *151*, 68. [[CrossRef](#)]
16. Slawson, R.W.; Prša, A.; Welsh, W.F.; Orosz, J.A.; Rucker, M.; Batalha, N.; Doyle, L.R.; Engle, S.G.; Conroy, K.; Coughlin, J.; et al. Kepler Eclipsing Binary Stars. II. 2165 Eclipsing Binaries in the Second Data Release. *Astron. J.* **2011**, *142*, 160. [[CrossRef](#)]
17. Stumpe, M.C.; Smith, J.C.; Van Cleve, J.E.; Twicken, J.D.; Barclay, T.S.; Fanelli, M.N.; Girouard, F.R.; Jenkins, J.M.; Kolodziejczak, J.J.; McCauliff, S.D.; et al. Kepler Presearch Data Conditioning I—Architecture and Algorithms for Error Correction in Kepler Light Curves. *Publ. Astron. Soc. Pac.* **2012**, *124*, 985. [[CrossRef](#)]
18. Luo, A.-L.; Zhao, Y.-H.; Zhao, G.; Deng, L.-C.; Liu, X.-W.; Jing, Y.-P.; Wang, G.; Zhang, H.-T.; Shi, J.-R.; Cui, X.-Q.; et al. The first data release (DR1) of the LAMOST regular survey. *Res. Astron. Astrophys.* **2015**, *15*, 1095–1124. [[CrossRef](#)]
19. Zhang, B.; Li, J.; Yang, F.; Xiong, J.-P.; Fu, J.-N.; Liu, C.; Tian, H.; Li, Y.-B.; Wang, J.-X.; Liang, C.-X.; et al. Self-consistent Stellar Radial Velocities from LAMOST Medium-resolution Survey DR7. *Astrophys. J. Suppl. Ser.* **2021**, *256*, 14. [[CrossRef](#)]
20. Tonry, J.; Davis, M. A survey of galaxy redshifts. I. Data reduction techniques. *Astron. J.* **1979**, *84*, 1511–1525. [[CrossRef](#)]
21. Nelder, J.A.; Mead, R. A Simplex Method for Function Minimization. *Comput. J.* **1965**, *7*, 308–313. [[CrossRef](#)]
22. Prša, A.; Zwitter, T. A Computational Guide to Physics of Eclipsing Binaries. I. Demonstrations and Perspectives. *Astrophys. J.* **2005**, *628*, 426–438. [[CrossRef](#)]
23. Prša, A.; Conroy, K.E.; Horvat, M.; Pablo, H.; Kochoska, A.; Bloemen, S.; Giammarco, J.; Hambleton, K.M.; Degroote, P. Physics of Eclipsing Binaries. II. Toward the Increased Model Fidelity. *Astrophys. J. Suppl. Ser.* **2016**, *227*, 29. [[CrossRef](#)]
24. Jones, D.; Conroy, K.E.; Horvat, M.; Giammarco, J.; Kochoska, A.; Pablo, H.; Brown, A.J.; Sowicka, P.; Prša, A. Physics of Eclipsing Binaries. IV. The Impact of Interstellar Extinction on the Light Curves of Eclipsing Binaries. *Astrophys. J. Suppl. Ser.* **2020**, *247*, 63. [[CrossRef](#)]
25. Hambleton, K.M.; Kurtz, D.W.; Prša, A.; Guzik, J.A.; Pavlovski, K.; Bloemen, S.; Southworth, J.; Conroy, K.; Littlefair, S.P.; Fuller, J. KIC 4544587: An eccentric, short-period binary system with δ Sct pulsations and tidally excited modes. *Mon. Not. R. Astron. Soc.* **2013**, *434*, 925–940. [[CrossRef](#)]
26. Wilson, R.E.; Devinney, E.J. Realization of Accurate Close-Binary Light Curves: Application to MR Cygni. *Astrophys. J.* **1971**, *166*, 605. [[CrossRef](#)]
27. Rasmussen, C.E.; Williams, C.K.I. *Gaussian Processes for Machine Learning*; MIT Press: Cambridge, MA, USA, 2006; ISBN 13-978-0-262-18253-9.

28. Wang, J.; Fu, J.; Niu, H.; Pan, Y.; Li, C.; Zong, W.; Hou, Y. KIC 5359678: A detached eclipsing binary with starspots. *Mon. Not. R. Astron. Soc.* **2021**, *504*, 4302–4311. [[CrossRef](#)]
29. Bressan, A.; Marigo, P.; Girardi, L.; Salasnich, B.; Cero, C.D.; Rubele, S.; Nanni, A. PARSEC: Stellar tracks and isochrones with the PAdova and TRieste Stellar Evolution Code. *Mon. Not. R. Astron. Soc.* **2012**, *427*, 127–145. [[CrossRef](#)]
30. Zong, W.; Charpinet, S.; Vauclair, G. Signatures of nonlinear mode interactions in the pulsating hot B subdwarf star KIC 10139564. *Astron. Astrophys.* **2016**, *594*, A46. [[CrossRef](#)]
31. Zong, W.; Charpinet, S.; Vauclair, G.; Giammichele, N.; Van Grootel, V. Amplitude and frequency variations of oscillation modes in the pulsating DB white dwarf star KIC 08626021. The likely signature of nonlinear resonant mode coupling. *Astron. Astrophys.* **2016**, *585*, A22. [[CrossRef](#)]
32. Holzwarth, V.; Schüssler, M. Dynamics of magnetic flux tubes in close binary stars. I. Equilibrium and stability properties. *Astron. Astrophys.* **2003**, *405*, 291–301. [[CrossRef](#)]
33. McQuillan, A.; Mazeh, T.; Aigrain, S. Rotation Periods of 34,030 Kepler Main-sequence Stars: The Full Autocorrelation Sample. *Astrophys. J. Suppl. Ser.* **2014**, *211*, 24. [[CrossRef](#)]
34. Basri, G.; Shah, R. The Information Content in Analytic Spot Models of Broadband Precision Light Curves. II. Spot Distributions and Lifetimes and Global and Differential Rotation. *Astrophys. J.* **2020**, *901*, 14. [[CrossRef](#)]
35. Wang, J.; Fu, J.; Zong, W.; Pan, Y.; Niu, H.; Zhang, B.; Zhang, Y. Properties and evolutions of starspots on three detached eclipsing binaries in the LAMOST-Kepler survey. *Mon. Not. R. Astron. Soc.* **2022**, *511*, 2285–2301. [[CrossRef](#)]
36. Pringle, J.E. Period changes in eruptive binaries. *Mon. Not. R. Astron. Soc.* **1975**, *170*, 633–642. [[CrossRef](#)]
37. Ma, X.Y.; Zong, W.; Fu, J.N.; Reed, M.D.; Wang, J.; Charpinet, S.; Su, J. K2 Photometry on Oscillation Mode Variability: The New Pulsating Hot B Subdwarf Star EPIC 220422705. *Astrophys. J.* **2022**, *933*, 211. [[CrossRef](#)]
38. Basri, G.; Streichenberger, T.; McWard, C.; Edmond, I.V.L.; Tan, J.; Lee, M.; Melton, T. A New Method for Estimating Starspot Lifetimes Based on Autocorrelation Functions. *Astrophys. J.* **2022**, *924*, 31. [[CrossRef](#)]

Disclaimer/Publisher’s Note: The statements, opinions and data contained in all publications are solely those of the individual author(s) and contributor(s) and not of MDPI and/or the editor(s). MDPI and/or the editor(s) disclaim responsibility for any injury to people or property resulting from any ideas, methods, instructions or products referred to in the content.